Supporting Information

Multiphysics analytical and numerical studies of biomolecule preconcentration utilizing ion concentration polarization: A case study of convergent microchannels

Van-Truong Dang[1], Van-Sang Pham[1,*]

[1] Hanoi University of Science and Technology, Hanoi, Vietnam

* Corresponding address: sang.phamvan@hust.edu.vn

Note 1. Analytical solutions of the simplified Poisson-Nernst-Planck-Navier-Stokes equations

The simplified Poisson-Nernst-Planck-Navier-Stokes equations are shown below:

$$\nabla.\mathbf{j}_i = 0 \tag{S1}$$

$$\mathbf{j}_i = -D_i\nabla c_i + \mu_i z_i c_i \mathbf{E} + \mathbf{u}c_i \tag{S2}$$

$$\nabla.\mathbf{u} = 0 \tag{S3}$$

$$-\nabla p + \eta\nabla^2\mathbf{u} + F\left(z_1c_1 + z_2c_2\right)\mathbf{E} = 0 \tag{S4}$$

$$\nabla^2\phi = -\frac{F\sum z_i c_i}{\varepsilon_0\varepsilon_r} \tag{S5}$$

To solve these equations, we use the following assumptions: (i) the condition of electroneutrality is satisfied in the whole domain, i.e., $z_1c_1 + z_2c_2 + z_Bc_B = 0$; (ii) the concentration of biomolecules is extremely dilute compared to the ones of the electrolyte solution (c_B ≪ c_1, c_2); and (iii) in the 2D model, the length scale is much larger than its wide scale; therefore, the flow is considered as unidirectional, i.e., $\partial u / \partial x = 0$ or $u = f(y)$.

In the model, the electric potentials are applied along the channel, and the width scale (y-direction) is much smaller than the length scale (x-direction); therefore, the tangential electric field E_x is roughly constant along the y-direction while the normal electric field E_y is nearly zero, except in the region near the channel wall. Therefore, the width-averaged tangential electric field $\bar{E}_x$ is approximately equal to the E_x, which is confirmed by the simulation, as shown in **Figures S1a, b**.

$$\bar{E}_x = \frac{1}{W}\int_W E_x dy = E_x \tag{S6}$$

$$E_y \approx 0 \tag{S7}$$

Similarly, the ion concentration varies along the x-direction but is nearly constant along the y-direction. In fact, the ion concentration changes rapidly toward the charged walls of the channel,

resulting in the formation of the electric double layer (EDL). With different ion concentrations of buffer solution of 10^{-3} mol m^{-3}, 10^{-2} mol m^{-3}, and 1 mol m^{-3}, the EDL thickness is approximately 300 nm, 100 nm, and 10 nm, respectively, as shown in **Figure S1c**. In this study, the width of the main channel is 20 μm; the channel-width/EDL ratio ($W/2\lambda_D$ as stated below) is approximately 33 to 1000, allowing the assumption of thin EDL. The width-averaged ion concentration $\overline{c}$ is then approximated by,

$$\overline{c} = \frac{1}{W}\int_W c\,dy = c \tag{S8}$$

From the conditions (S6), (S7), and (S8) and based on Eq. (S2), the y-direction molar flux j_y is zero approximately, while all elements of the x-direction molar flux are independent of the y-direction, but not the last element, which contains the velocity u. Therefore, the molar flux equals the x-direction molar flux, i.e., $j = j_x$ as shown in **Figure S1d**. From Eq. (S1), we obtain

$$\frac{\mathrm{d}j_i}{\mathrm{d}x} = \frac{\mathrm{d}j_{x,i}}{\mathrm{d}x} = 0 \tag{S9}$$

The width-averaged molar flux is determined by

$$\overline{j}_i = \frac{1}{W}\int_W j_i \mathrm{d}y = \frac{1}{W}\int_W -D_i\frac{\mathrm{d}c_i}{\mathrm{d}x}\mathrm{d}y + \frac{1}{W}\int_W \mu_i z_i c_i E_x \mathrm{d}y + \frac{1}{W}\int_W u c_i \mathrm{d}y \tag{S10}$$

Notice that

$$\frac{1}{W}\int_W u c_i \mathrm{d}y = \frac{1}{W}\left(c_i\int_W u\mathrm{d}y - \int_W c_{i,y}\left(\int_W u\mathrm{d}y\right)\mathrm{d}y\right) = c_i\frac{1}{W}\int_W u\mathrm{d}y = c_i\overline{u} = \overline{c}_i\overline{u} \tag{S11}$$

Therefore, Eq. (S10) becomes

$$\overline{j}_i = -D_i\frac{\mathrm{d}\overline{c}_i}{\mathrm{d}x} + \mu_i z_i \overline{c}_i \overline{E}_x + \overline{c}_i\overline{u} \tag{S12}$$

or

$$\frac{\overline{j}_i}{\mu_i} = -\frac{D_i}{z_i\mu_i}\frac{\mathrm{d}z_i\overline{c}_i}{\mathrm{d}x} + z_i\overline{c}_i\overline{E}_x + \frac{z_i\overline{c}_i}{z_i\mu_i}\overline{u} \tag{S13}$$

From the assumption (i), $z_1\overline{c}_1 + z_2\overline{c}_2 = 0$, we set $z_1\overline{c}_1 = -z_2\overline{c}_2 = \overline{c}$, and Eq. (S13) becomes

$$\frac{\overline{j}_1}{\mu_1} = -\frac{D_1}{z_1\mu_1}\frac{\mathrm{d}\overline{c}}{\mathrm{d}x} + \overline{c}\overline{E}_x + \frac{\overline{c}}{z_1\mu_1}\overline{u} \tag{S14}$$

$$\frac{\overline{j}_2}{\mu_2} = \frac{D_2}{z_2\mu_2}\frac{\mathrm{d}\overline{c}}{\mathrm{d}x} - \overline{c}\overline{E}_x - \frac{\overline{c}}{z_2\mu_2}\overline{u} \tag{S15}$$

Adding Eq. (S14) to (S15), and combining with Eq. (S9), we obtain

$$\frac{\mathrm{d}}{\mathrm{d}x}\left(\frac{\overline{j}_1}{\mu_1}\right) + \frac{\mathrm{d}}{\mathrm{d}x}\left(\frac{\overline{j}_2}{\mu_2}\right) = \frac{\mathrm{d}}{\mathrm{d}x}\left(-\left(\frac{D_1}{z_1\mu_1} - \frac{D_2}{z_2\mu_2}\right)\frac{\mathrm{d}\overline{c}}{\mathrm{d}x} + \overline{u}\left(\frac{1}{z_1\mu_1} - \frac{1}{z_2\mu_2}\right)\overline{c}\right) = 0 \tag{S16}$$

Equation (S16) is solved analytically with appropriate boundary conditions: (i) $\overline{c} = c_0$ at the channel inlet ($x = 0$), and (ii) $\overline{c} = 0$ at the position of the ion depletion zone ($x = L$), and the analytical solution $\overline{c}$ is

$$\frac{\overline{c}}{c_0} = \frac{c}{c_0} = \frac{1 - \exp\left[\frac{\overline{u}}{D_{eff}}(x - L)\right]}{1 - \exp\left[-\frac{\overline{u}L}{D_{eff}}\right]} \tag{S17}$$

where D_{eff} is the effective diffusivity defined by $D_{eff} = \left(D_2 z_1 \mu_1 - D_1 z_2 \mu_2\right) / \left(z_1 \mu_1 - z_2 \mu_2\right)$.

The ionic current generated by the motion of the charged species is given by

$$I = FW \sum z_i \overline{j}_i = FW \left(-\left(D_1 - D_2\right) \frac{\mathrm{d}\overline{c}}{\mathrm{d}x} + \left(z_1 \mu_1 - z_2 \mu_2\right) \overline{c} \overline{E}_x \right) \tag{S18}$$

where W is the width of the channel.

Using Eq. (S17) and rearranging Eq. (S18), we obtain the $\overline{E}_x$ as

$$\begin{aligned} \overline{E}_x = E_x = &-\frac{D_1 - D_2}{z_1 \mu_1 - z_2 \mu_2} \frac{\overline{u}}{D_{eff}} \frac{\exp\left(\frac{\overline{u}}{D_{eff}}(x - L)\right)}{1 - \exp\left(\frac{\overline{u}}{D_{eff}}(x - L)\right)} + \\ &+ \frac{I}{FWc_0\left(z_1 \mu_1 - z_2 \mu_2\right)} \frac{1 - \exp\left(-\frac{\overline{u}L}{D_{eff}}\right)}{1 - \exp\left(\frac{\overline{u}}{D_{eff}}(x - L)\right)} \end{aligned} \tag{S19}$$

However, as stated above, there is the electric double layer near the charged wall surface, which generates the supplement electric potential ψ satisfied the following boundary conditions:

$$\begin{aligned} &\psi = \psi_s \ \text{at} \ y = W/2 \ (\text{at the wall surface}) \\ &\psi = 0 \ \text{at location far from wall surface} \end{aligned} \tag{S20}$$

where ψ_s is the surface potential.

Based on the Gouy-Chapman theory, the potential ψ is determined by

$$\psi = \frac{2}{\frac{ze}{k_B T}} \ln\left(\frac{1 + \exp\left(-\frac{W/2 - y}{\lambda_D}\right) \tanh\left(\frac{ze\psi_s}{4k_B T}\right)}{1 - \exp\left(-\frac{W/2 - y}{\lambda_D}\right) \tanh\left(\frac{ze\psi_s}{4k_B T}\right)} \right) \tag{S21}$$

where λ_D is the Debye length, which is calculated by,

$$\lambda_D = \sqrt{\frac{\varepsilon_0 \varepsilon_r k_B T}{e^2 \sum_{i=1}^{N} z_i^2 N_A c_0}} \tag{S22}$$

Differentiating ψ of Eq. (S21) with respect to y, we obtain the supplement electric field,

$$E_{s,x} = -\frac{d\psi}{dy} = -\frac{4k_B T}{ze\lambda_D} \frac{\exp\left(-\frac{W/2-y}{\lambda_D}\right)\tanh\left(\frac{ze\psi_s}{4k_B T}\right)}{\left(1-\exp\left(-\frac{W/2-y}{\lambda_D}\right)\tanh\left(\frac{ze\psi_s}{4k_B T}\right)\right)\left(1+\exp\left(-\frac{W/2-y}{\lambda_D}\right)\tanh\left(\frac{ze\psi_s}{4k_B T}\right)\right)} \tag{S23}$$

Similarly, there is the supplement ionic concentration in the electric double layer, which is determined by the Boltzmann distribution,

$$\frac{c_{s,i}}{c_0} = \exp\left(-\frac{z_i e\psi}{k_B T}\right) \tag{S24}$$

Substituting Eq. (S21) into Eq. (S24), we obtain

$$\frac{c_{s,i}}{c_0} = \left(\frac{1-\exp\left(-\frac{W/2-y}{\lambda_D}\right)\tanh\left(\frac{ze\psi_s}{4k_B T}\right)}{1+\exp\left(-\frac{W/2-y}{\lambda_D}\right)\tanh\left(\frac{ze\psi_s}{4k_B T}\right)}\right)^{2i} \tag{S25}$$

where i = 1 for cations, and i = -1 for anions.

Combining Eq. (S17) and Eq. (S.25) with the notice that the bulk ionic concentration was calculated twice in these equations, the ionic concentration distribution for 2D models is generally determined by

$$\frac{c_i}{c_0} = \frac{1-\exp\left[\frac{\overline{u}}{D_{eff}}(x-L)\right]}{1-\exp\left[-\frac{\overline{u}L}{D_{eff}}\right]} + \left(\frac{1-\exp\left(-\frac{W/2-y}{\lambda_D}\right)\tanh\left(\frac{ze\psi_s}{4k_B T}\right)}{1+\exp\left(-\frac{W/2-y}{\lambda_D}\right)\tanh\left(\frac{ze\psi_s}{4k_B T}\right)}\right)^{2i} - 1 \tag{S26}$$

The tangential electric field is also calculated by Eq. (S19) and Eq. (S23) for 2D models,

$$E_x = -\frac{D_1 - D_2}{z_1\mu_1 - z_2\mu_2}\frac{\overline{u}}{D_{eff}}\frac{\exp\left(\frac{\overline{u}}{D_{eff}}(x-L)\right)}{1-\exp\left(\frac{\overline{u}}{D_{eff}}(x-L)\right)} + \frac{I}{FWc_0(z_1\mu_1 - z_2\mu_2)}\frac{1-\exp\left(-\frac{\overline{u}L}{D_{eff}}\right)}{1-\exp\left(\frac{\overline{u}}{D_{eff}}(x-L)\right)} \tag{S27}$$

$$-\frac{4k_B T}{ze\lambda_D}\frac{\exp\left(-\frac{W/2-y}{\lambda_D}\right)\tanh\left(\frac{ze\psi_s}{4k_B T}\right)}{\left(1-\exp\left(-\frac{W/2-y}{\lambda_D}\right)\tanh\left(\frac{ze\psi_s}{4k_B T}\right)\right)\left(1+\exp\left(-\frac{W/2-y}{\lambda_D}\right)\tanh\left(\frac{ze\psi_s}{4k_B T}\right)\right)}$$

Equations (S26) and (S27) are applied for the symmetric (z : z) electrolyte solution. When the surface potential is small (ψ_s << 0.025 V), the electric potential ψ_s is simplified by the following solution,

$$\psi = \psi_s \exp\left(-\frac{W/2-y}{\lambda_D}\right) \tag{S28}$$

Equation (S28) refers to the Debye-Huckel approximation. Differentiating ψ of Eq. (S28) with respect to y obtains the supplement electric field,

$$E_{s,x} = -\frac{\mathrm{d}\psi}{\mathrm{d}y} = -\frac{\psi_s}{\lambda_D}\exp\left(-\frac{W/2-y}{\lambda_D}\right) \tag{S29}$$

And the supplement ionic concentration in the electric double layer is determined by,

$$\frac{c_{s,i}}{c_0} = \exp\left(-\frac{z_i e\psi}{k_B T}\right) = \exp\left(-\frac{z_i e\psi_s}{k_B T}\exp\left(-\frac{W/2-y}{\lambda_D}\right)\right) \tag{S30}$$

Therefore, the ionic concentration distribution and the tangential electric field for 2D models in cases of low surface potentials with both symmetric and asymmetric electrolyte solutions are respectively described by

$$\frac{c_i}{c_0} = \frac{1-\exp\left[\frac{\overline{u}}{D_{eff}}(x-L)\right]}{1-\exp\left[-\frac{\overline{u}L}{D_{eff}}\right]} + \exp\left(-\frac{z_i e\psi_s}{k_B T}\exp\left(-\frac{W/2-y}{\lambda_D}\right)\right) - 1 \tag{S31}$$

$$E_x = -\frac{D_1-D_2}{z_1\mu_1 - z_2\mu_2}\frac{\overline{u}}{D_{eff}}\frac{\exp\left(\frac{\overline{u}}{D_{eff}}(x-L)\right)}{1-\exp\left(\frac{\overline{u}}{D_{eff}}(x-L)\right)} + \frac{I}{FWc_0(z_1\mu_1 - z_2\mu_2)}\frac{1-\exp\left(-\frac{\overline{u}L}{D_{eff}}\right)}{1-\exp\left(\frac{\overline{u}}{D_{eff}}(x-L)\right)} \tag{S32}$$
$$-\frac{\psi_s}{\lambda_D}\exp\left(-\frac{W/2-y}{\lambda_D}\right)$$

Equations (S26), (S27), (S31), and (S32) are applied for 2D models in a region far from the IDZ but still provide acceptable solutions close to the IDZ boundary where the non-linear depletion of ions makes the electric field magnified significantly, leading the formation of vortices in this region. The validation is presented in section 5.1 in the main text.

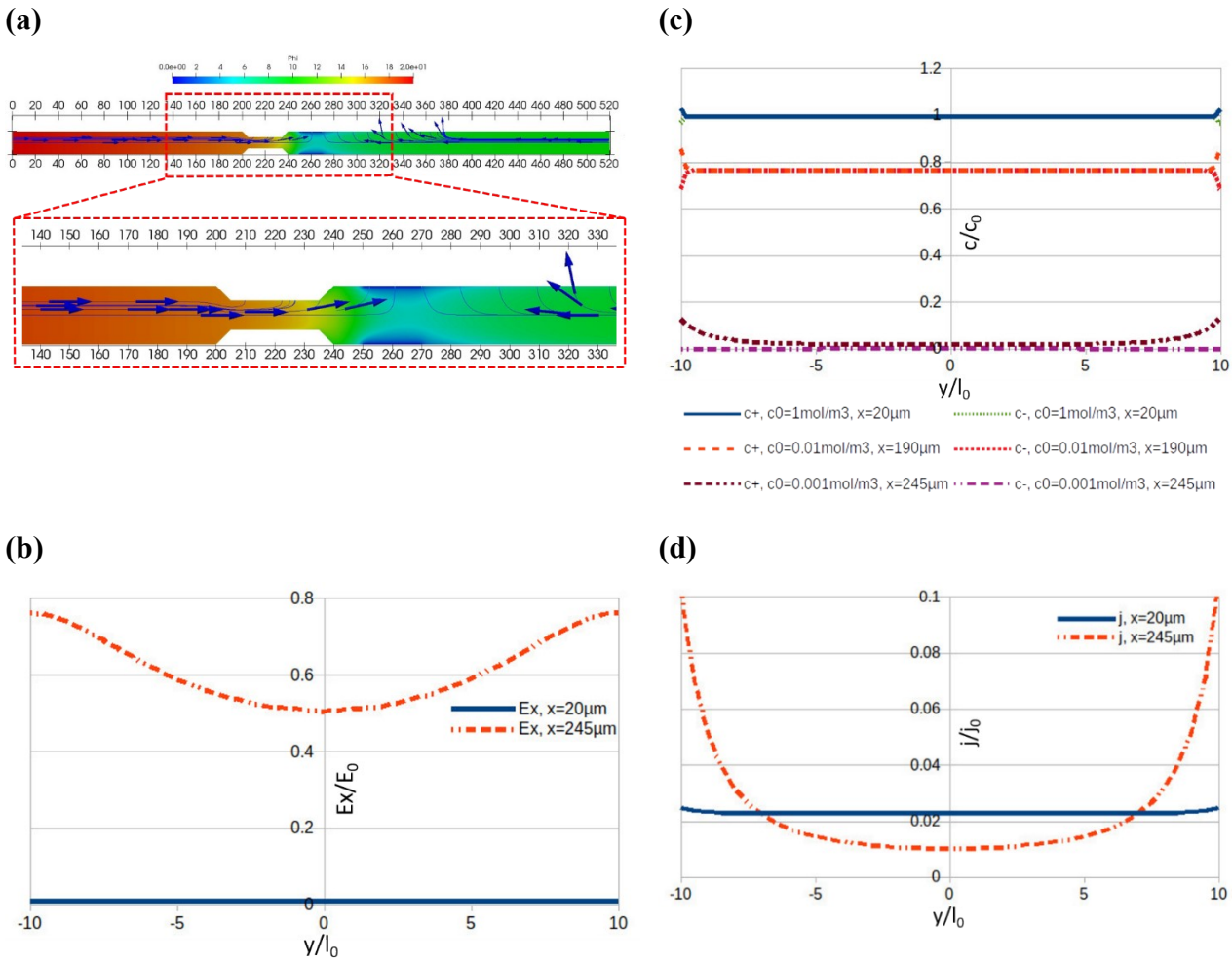

Figure S1. The numerical simulations of the 20 μm-main channel-width model with the convergent width of 10 μm under the application of external potentials of $V_H = 20V_0$ and $V_L = 10V_0$: **(a)** the electric field in the channel; **(b)** the tangential electric fields along the *y*-direction far from the IDZ (x = 20 μm) and in the IDZ (x = 245 μm), respectively; **(c)** the ion concentrations along the *y*-direction with different ion concentrations of buffer solution at various sections of the channel; **(d)** the ionic fluxes along the *y*-direction far from the IDZ (x = 20 μm) and in the IDZ (x = 245 μm), respectively. At the position of x = 245 μm, the ion concentration decreases sharply due to the nonlinear electroconvective instability, making the electric field increase significantly, while the total ionic flux is conserved from the channel inlet to the ion-selective membrane. These parameters vary slightly along the *y*-direction in the bulk region but relatively in the IDZ.

Note 2. Validation for analytical and numerical simulation results

In this work, we introduce the simplified analytical model to verify numerical simulations and experimental results of actual models. To validate solutions obtained from numerical simulations using this analytical model, we examine two cases: (i) the 20 μm main-channel-width model with a convergent width of 10 μm and (ii) the 20 μm straight-channel-width model. Both models are applied by external electric potentials of $V_H = 20V_0$ and $V_L = 10V_0$ at the electrodes while the ion-selective membrane is connected to the ground. In the analytical model, the ionic current I, the flow velocity u, and the position of the ion depletion zone L are determined from simulations or experiments. By using numerical results, these parameters are $I = 0.474i_0 = 0.912\times10^{-7}$ A/m, $I = 0.533i_0 = 1.026\times10^{-7}$ A/m; $L = 237$ μm, $L = 237$ μm, and the profile of velocities u are shown in **Figures S2a, b** for case (i) and (ii), respectively. The results show that the solution acquired from analytical solutions and the ones from numerical simulations are highly consistent for both cases, except for a slight difference in a convergent sector of the convergent channel model, as indicated in Section 5.1 in the main text.

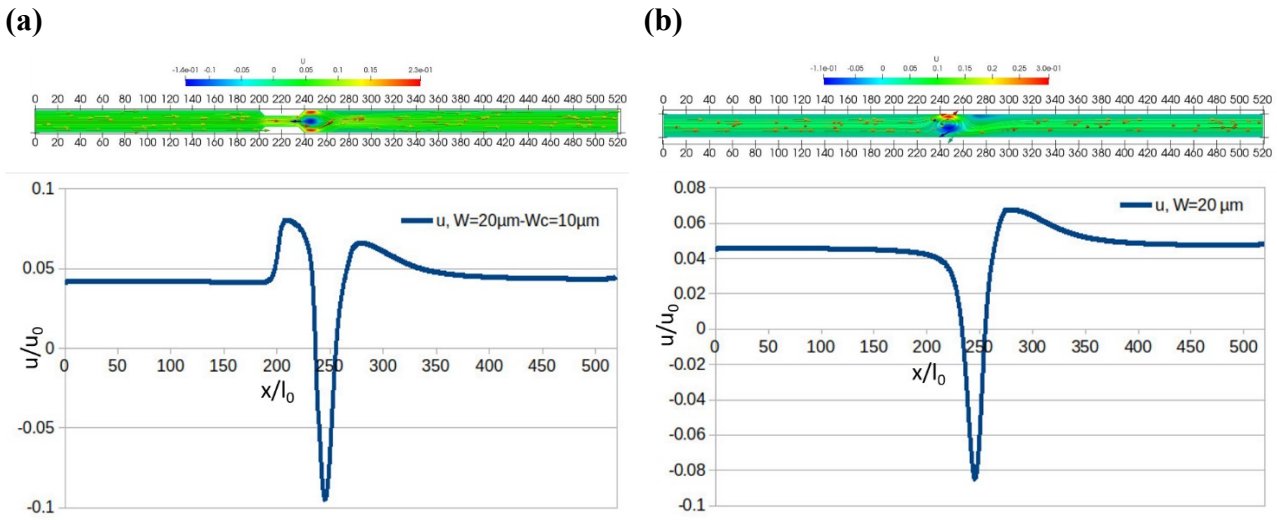

Figure S2. The profiles of velocities along the channel in two cases. **(a)** The 20 μm main-channel-width model with a convergent width of 10 μm; **(b)** The 20 μm straight-channel-width model. Both models are applied by external electric potentials of $V_H = 20V_0$ and $V_L = 10V_0$ at the electrodes while the ion-selective membrane is connected to the ground.

Note 3. Utilizing the analytical model to determine the critical width of the convergent sector in the channel

In the main text, under the application of electric potentials of $V_H = 20V_0$ and $V_L = 10V_0$, the 20 μm-width main channel must have a convergent width larger than 2.5 μm to ensure the preconcentration of biomolecules located into the convergent sector of the channel. This numerical critical width is also confirmed by the analytical model.

To validate the minimum width obtained by simulation, we examine it using Eq. (24) in the main text. From the simulation results, under the established working parameters above, the channel embedded with a 2.5 μm-width convergent sector has the ionic current $I = 0.228i_0 = 0.439\times10^{-7}$ A/m, the width-averaged velocity at the starting point of the convergent sector $\overline{u} = 0.1161u_0 = 0.617\times10^{-4}$ m/s, the maximum velocity at the starting point of the convergent sector $u_m = 0.171u_0 = 0.91\times10^{-4}$ m/s, and the position of the IDZ $L = 215$ μm, and the starting point of the convergent sector $L_1 = 205$ μm, as shown in **Figure S3**. If the convergent channel has such parameters, its width must be satisfied Eq. (24) in the main text,

$$W_{c,\min} = \frac{I\left(1-\exp\left(-\frac{\overline{u}_c L}{D_{eff}}\right)\right)}{Fc_0\left(z_1\mu_1 - z_2\mu_2\right)}\left(\frac{u_m}{\mu_B} - \left(\frac{u_m}{\mu_B} - \frac{D_1 - D_2}{z_1\mu_1 - z_2\mu_2}\frac{\overline{u}}{D_{eff}}\right)\exp\left(-\frac{\overline{u}}{D_{eff}}\left(L - L_1\right)\right)\right)^{-1}$$

Substituting I, $\overline{u}$, u_m, L, and L_1 into this equation, we obtain $W_{min} = 1.92$ μm.

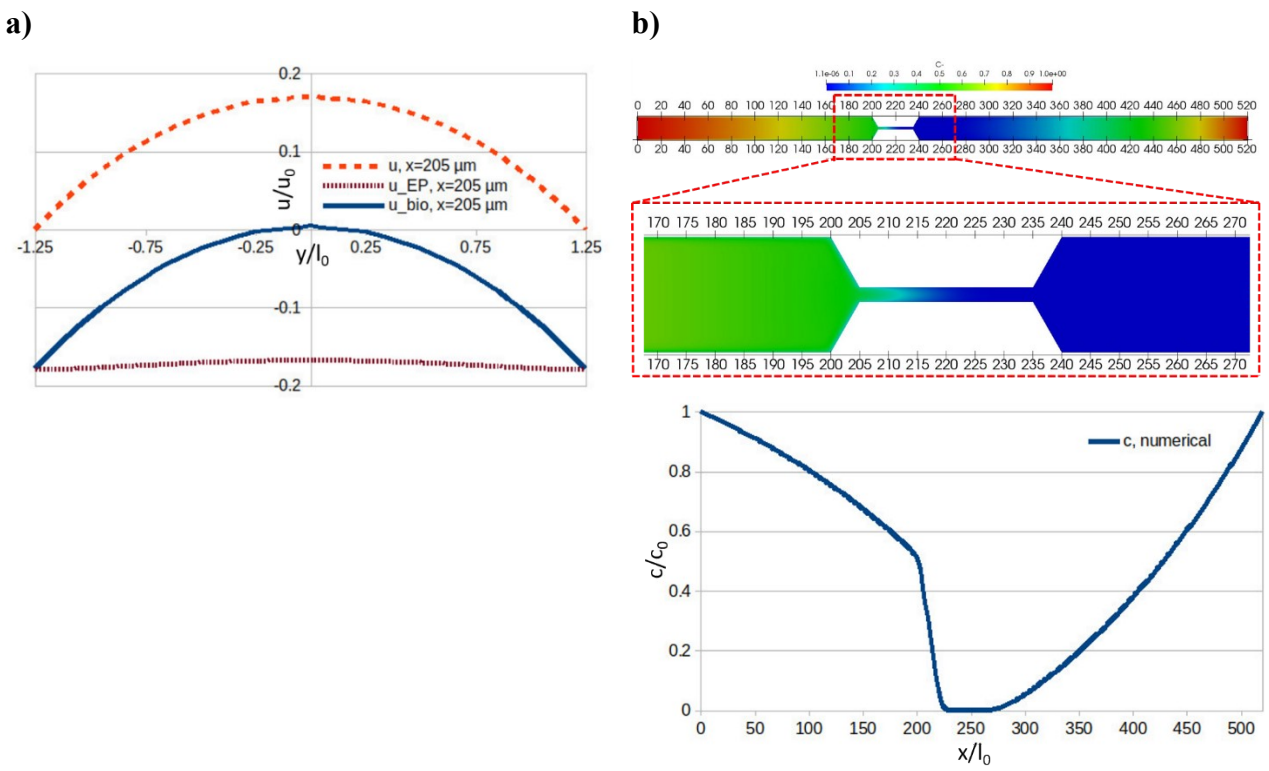

Figure S3. **(a)** The profile of the biomolecule velocity along the *y*-axis at the starting point of the convergent sector (x = 205 µm); **(b)** The distribution of ion concentration along the channel (y = 0 µm). These results are used to determine the minimum width using the analytical model to validate the numerical critical dimension of the convergent sector.

Note 4. Determining positions of the ion-selective membrane to ensure biomolecules preconcentrate in the convergent sector of the channel

In the main text, the farthest and nearest positions of the ion-selective membrane for biomolecules preconcentrated in the convergent sector of the channel are determined numerically with values of 292.5 μm and 248 μm, respectively. These results could also be calculated by analytical Eqs. (25) and (26) in the main text.

As mentioned in the main text, the position L of the ion-selective membrane is indirectly calculated through the position of the IDZ with the assumption that these two positions are close enough to each other. This assumption depends on many conditions, especially on the channel width. As indicated in Section 5.3 in the main text, when the channel width decreases, the fluid flow decreases as well, making the slow flux of ions in the channel. When the ions are depleted in the IDZ, they are supplied from the bulk flow far from the ion-selective membrane. The ion supplement speed significantly depends on the bulk flow. In addition, when the width of the channel gets narrower, there are fewer ions in the area around the ion-selective membrane. Both conditions make the IDZ expand towards the entrance when the channel width reduces. Therefore, to ensure the condition of coincidence between the position of the ion-selective membrane and the one of the IDZ, we must examine these positions according to the ratio $W/2\lambda_D$. From **Figure S4** and **Table S1**, the difference between the two positions is acceptable when $W/2\lambda_D \geq 16.7$.

We consider the 20 μm-width main channel integrated with the convergent width W_c of 10 μm. The ending point (L_2) of the convergent sector is 235 μm from the entrance. Under the application of electric potentials of $V_H = 20V_0$ and $V_L = 10V_0$, the ionic current $I = 0.467i_0 = 0.899\times10^{-7}$ A/m, the width-averaged velocity at the ending point of the convergent sector $\overline{u} = 0.0575u_0 = 0.306\times10^{-4}$ m/s, the maximum velocity at the ending point of the convergent sector $u_m = 0.0772u_0 = 0.411\times10^{-4}$ m/s as shown in **Figure S5a**. The farthest position of the ion-selective membrane is calculated by Eq. (26),

$$L_{\max} = \frac{1}{-\dfrac{\overline{u}}{D_{eff}}} \ln\left(\frac{\dfrac{u_m}{\mu_B} - \dfrac{I}{FW_c c_0 \left(z_1\mu_1 - z_2\mu_2\right)}}{\left(\dfrac{u_m}{\mu_B} - \dfrac{D_1 - D_2}{z_1\mu_1 - z_2\mu_2} \dfrac{\overline{u}}{D_{eff}} \right) \exp\left(\dfrac{\overline{u}L_2}{D_{eff}} \right) - \dfrac{I}{FW_c c_0 \left(z_1\mu_1 - z_2\mu_2\right)}} \right)$$

Substituting I, $\overline{u}$, u_m, W_c, and L_2 into this equation, we obtain $L_{max} = 270.7$ μm.

Similarly, the 20 μm-width main channel integrated with the convergent sector at the starting point of $L_1 = 225$ μm has the ionic current $I = 0.607i_0 = 1.168\times10^{-7}$ A/m, the width-averaged velocity at the starting point $\overline{u} = 0.101u_0 = 0.537\times10^{-4}$ m/s, the maximum velocity at the ending point u_m =

$0.127u_0$ = 0.676×10^{-4} m/s as shown in **Figure S5b**. The nearest position of the ion-selective membrane is calculated by Eq. (25),

$$L_{\min} = \frac{1}{-\frac{\overline{u}}{D_{eff}}} \ln\left(\frac{\frac{u_m}{\mu_B} - \frac{I}{FW_c c_0 \left(z_1\mu_1 - z_2\mu_2\right)}}{\left(\frac{u_m}{\mu_B} - \frac{D_1 - D_2}{z_1\mu_1 - z_2\mu_2}\frac{\overline{u}}{D_{eff}}\right)\exp\left(\frac{\overline{u}L_1}{D_{eff}}\right) - \frac{I}{FW_c c_0 \left(z_1\mu_1 - z_2\mu_2\right)}} \right)$$

Substituting I, $\overline{u}$, u_m, W_c, and L_2 into this equation, we obtain L_{min} = 240.4 μm. Compared to the simulation (L_{min} = 248 μm), the analytical and numerical solutions agree with each other qualitatively.

Table S1. The IDZ and ion-selective membrane positions are compared according to the channel widths.

W (μm)	IDZ position (μm)	Ion-selective membrane position (μm)	Difference (%)	$W/2\lambda_D$
2	215	250	14	3.3
4	225	250	10	6.7
6	230	250	8	10
8	235	250	6	13.3
10	237	250	5.2	16.7
12	237	250	5.2	20

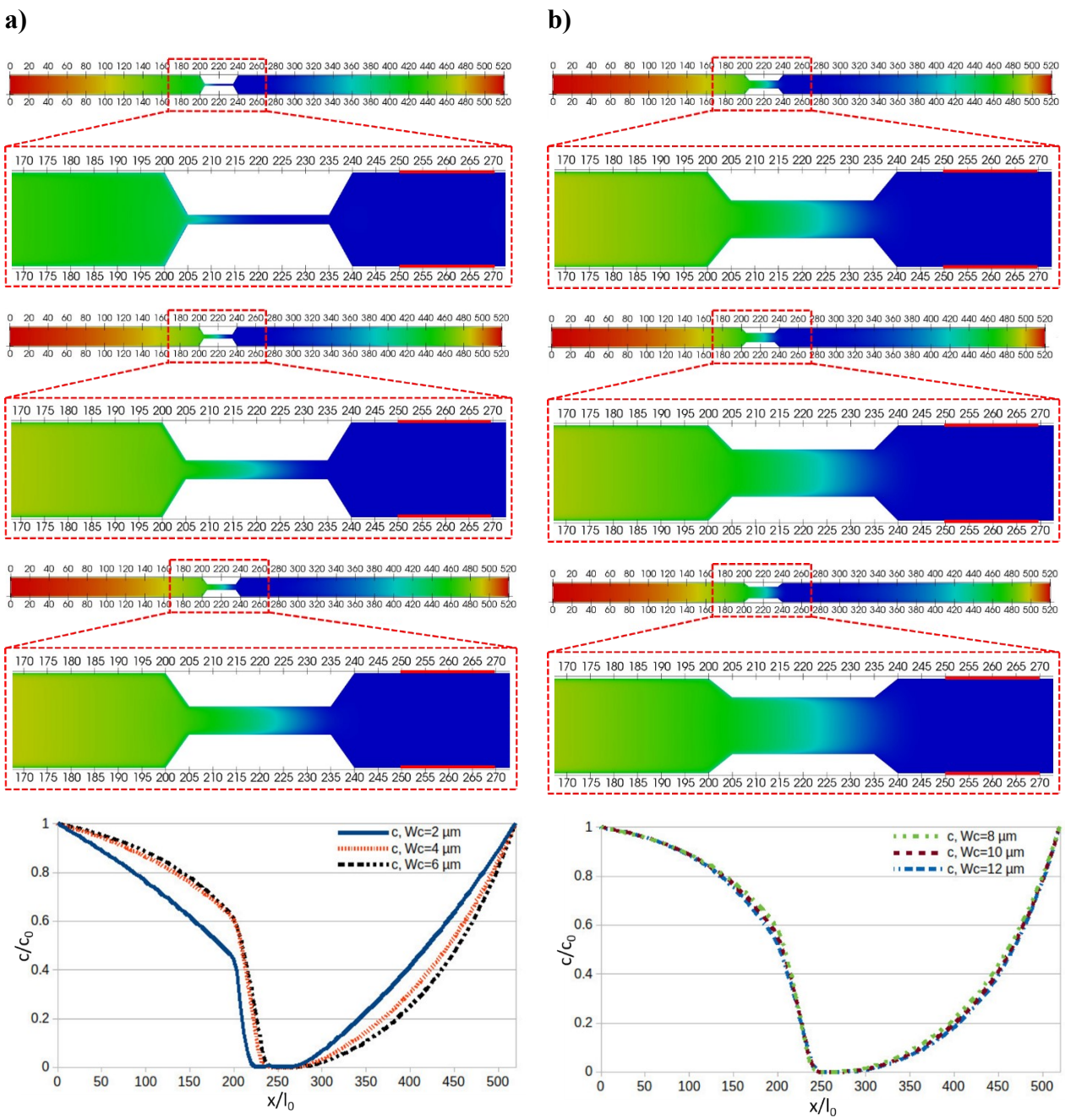

Figure S4. The position of the IDZ depends on the convergent width of the channel. **a)** The positions of the IDZ and the ion concentration distributions along the *x*-axis corresponding to the convergent widths of 2 μm, 4 μm, and 6 μm; **b)** The positions of the IDZ and the ion concentration distributions along the *x*-axis corresponding to the convergent widths of 8 μm, 10 μm, and 12 μm.

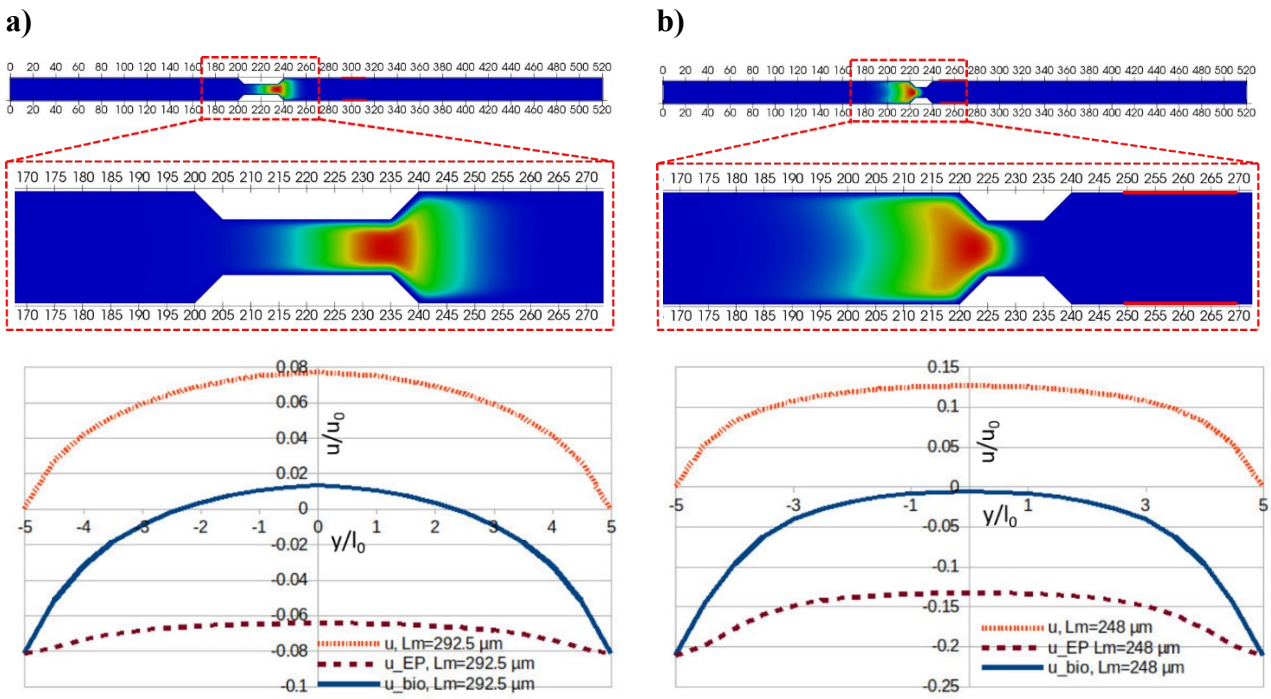

Figure S5. Determining positions of the ion-selective membrane to ensure biomolecules preconcentrate in the convergent sector of the channel. **a)** The preconcentration of biomolecules in the channel and the velocities along the *y*-axis at the ending point of the convergent sector (x = 235 µm) when the ion-selective membrane is 57.5 µm far from the ending point of the convergent sector. **b)** The preconcentration of biomolecules in the channel and the velocities along the *y*-axis at the starting point of the convergent sector (x = 225 µm) when the ion-selective membrane is 23 µm far from the starting point of the convergent sector.

Note 5. Utilizing the analytical model to determine critical pressures applied on the inlet of microchannels

As mentioned in the main text, biomolecules cannot preconcentrate in the convergent sector of the channel integrated with the 2 μm width convergent channel under the application of electric potentials of $V_H = 20V_0$ and $V_L = 10V_0$. This is due to the convergent width below the critical width for preconcentration in the convergent sector. From the simulation, if a minimum pressure of $4p_0$ is applied at the channel inlet, the preconcentrated biomolecule plug will migrate into the convergent region of the channel. This critical pressure could also be calculated using Eq. (34) in the main text. In **Figure S6b**, the electric field at the preconcentrated plug is $E_x = 0.109E_0 = 0.282 \times 10^4$ V/m, and the zeta potential of the channel wall is ζ = -20 mV. Substituting these values into Eq. (34),

$$p_{1,\min} = \left(\frac{\left(W_c/2\right)^2}{2\eta} \right)^{-1} \left(\mu_B + \frac{\varepsilon_0 \varepsilon_r \zeta}{\eta} \left(1 - \frac{1}{\cosh\left(W_c/2\lambda_D\right)} \right) \right) E_{x|x=L_1} L_c$$

We obtain $p_{1,min} = 4.6p_0$.

Similarly, the maximum pressure applied at the channel inlet to ensure biomolecules do not leak out the convergent sector is determined by Eq. (35) in the main text,

$$p_{1,\max} = \left(\frac{\left(W_c/2\right)^2}{2\eta} \right)^{-1} \left(\mu_B + \frac{\varepsilon_0 \varepsilon_r \zeta}{\eta} \left(1 - \frac{1}{\cosh\left(W_c/2\lambda_D\right)} \right) \right) E_{x|x=L_2} L_c$$

The parameters used in this equation are $E_x = 0.63E_0 = 1.63 \times 10^4$ V/m and ζ = -20 mV; we obtain the result $p_{1,max} = 26.5p_0$, which is consistent with the numerical solution of $p_{1,max} = 22p_0$.

The critical pressures depend significantly on the channel width, as indicated in Eqs. (34), (35). To the channel integrated with the 10 μm-width convergent sector under the same working conditions, the maximum pressure applied at the channel inlet is only $1p_0$, which is acquired from the simulation. This maximum pressure is also analytically calculated with $p_{1,max} = 0.5p_0$. The parameters used in this equation are $E_x = 0.326E_0 = 0.843 \times 10^4$ V/m and ζ = -20 mV, as shown in **Figure S6b**.

It is noticed that Eqs. (34) and (35) are applied for straight channels. However, the pressure changes significantly only in the convergent sector of the channel where the IDZ is formed, as shown in **Figure. 10a** in the main text. Therefore, these equations could be utilized for convergent channels, and results are solved in the convergent region with the length L_c = 30 μm, which is the main parameter in Eqs. (34), (35).

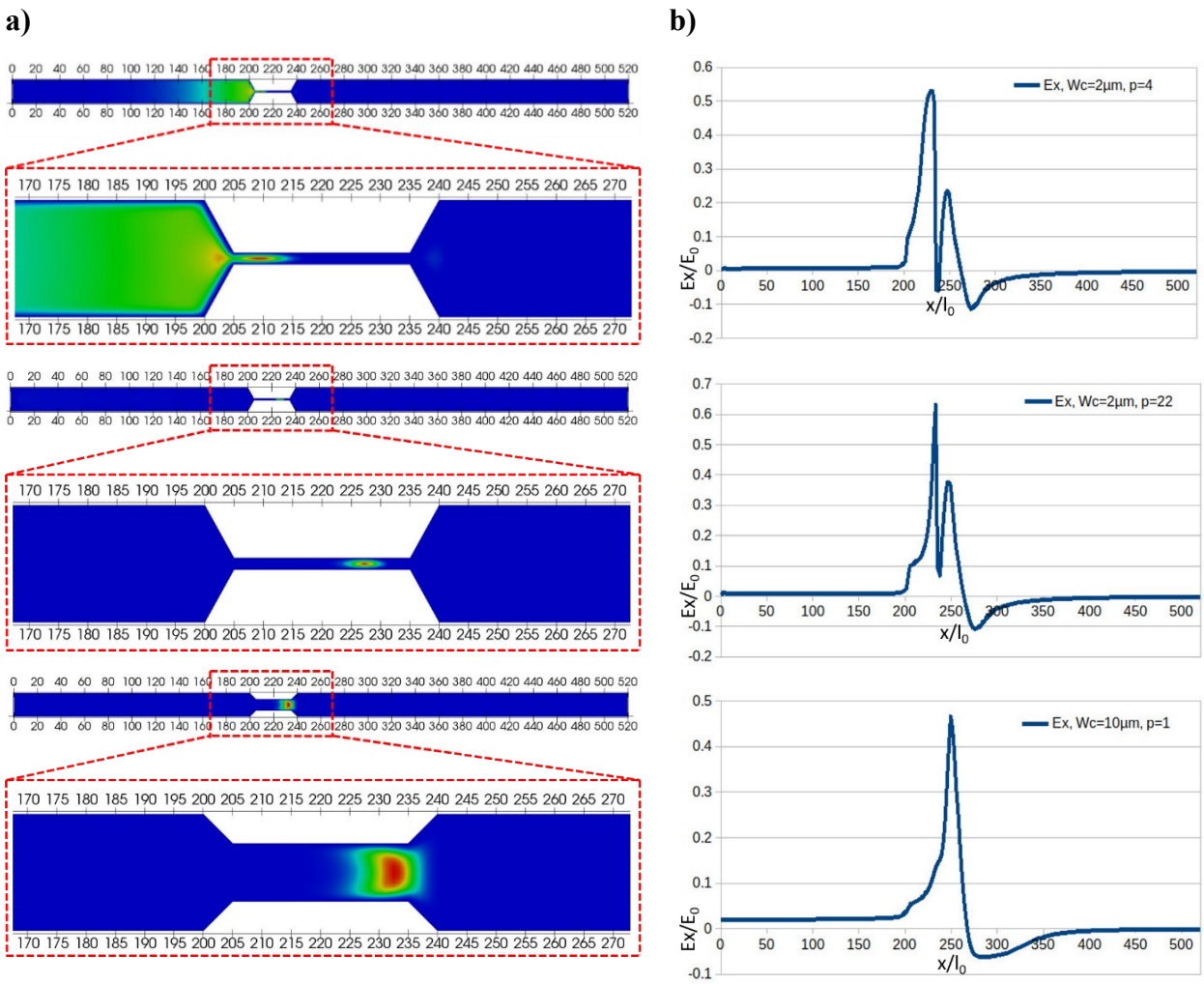

Figure S6. Determining critical external pressures applied at the channel inlet to ensure biomolecules preconcentrate in the convergent sector of the channel. **a)** Preconcentrations of biomolecules in the channels under the applications of critical external pressures. **b)** The electric fields correspond to the external pressures of $4p_0$, $22p_0$, and $1p_0$ applied at the channel inlet of 2 μm width convergent channels and the 10 μm width convergent channel.

REFERENCES

[1] A. T. K. Perera, D. T. Phan, S. Pudasaini, Y. Liu, and C. Yang, "Enhanced sample pre-concentration by ion concentration polarization on a paraffin coated converging microfluidic paper based analytical platform," *Biomicrofluidics*, vol. 14, no. 1, 2020, doi: 10.1063/1.5133946.

[2] C. L. Chen and R. J. Yang, "Effects of microchannel geometry on preconcentration intensity in microfluidic chips with straight or convergent-divergent microchannels," *Electrophoresis*, vol. 33, no. 5, pp. 751–757, 2012, doi: 10.1002/elps.201100493.

[3] C. C. Chao, P. H. Chiu, and R. J. Yang, "Preconcentration of diluted biochemical samples using microchannel with integrated nanoscale Nafion membrane," *Biomed. Microdevices*, vol. 17, no. 2, 2015, doi: 10.1007/s10544-015-9940-2.

[4] P. H. Chiu, C. H. Weng, and R. J. Yang, "Preconcentration and separation of mixed-species samples near a nano-junction in a convergent microchannel," *Sensors (Switzerland)*, vol. 15, no. 12, pp. 30704–30715, 2015, doi: 10.3390/s151229824.

[5] Y. Y. Chen, P. H. Chiu, C. H. Weng, and R. J. Yang, "Preconcentration of diluted mixed-species samples following separation and collection in a micro-nanofluidic device," *Biomicrofluidics*, vol. 10, no. 1, 2016, doi: 10.1063/1.4942037.

[6] R.-J. Yang, H.-H. Pu, and H.-L. Wang, "Ion concentration polarization on paper-based microfluidic devices and its application to preconcentrate dilute sample solutions," *Biomicrofluidics*, vol. 9, no. 1, pp. 1–12, Jan. 2015, doi: 10.1063/1.4913366.

[7] W. Ouyang, Z. Li, and J. Han, "Pressure-Modulated Selective Electrokinetic Trapping for Direct Enrichment, Purification, and Detection of Nucleic Acids in Human Serum," *Anal. Chem.*, vol. 90, no. 19, pp. 11366–11375, Oct. 2018, doi: 10.1021/acs.analchem.8b02330.

[8] V.-T. Dang and V.-S. Pham, "A numerical study of sample preconcentration using ion concentration polarization in single microfluidic channels with dual ion-selective membranes," *AIP Adv.*, vol. 13, no. 9, Sep. 2023, doi: 10.1063/5.0161190.

[9] V.-B. Nguyen, Q.-V. Do, and V.-S. Pham, "An OpenFOAM solver for multiphase and turbulent flow," *Phys. Fluids*, vol. 32, no. 4, Apr. 2020, doi: 10.1063/1.5145051.

[10] V. S. Pham, Z. Li, K. M. Lim, J. K. White, and J. Han, "Direct numerical simulation of electroconvective instability and hysteretic current-voltage response of a permselective membrane," *Phys. Rev. E*, vol. 86, no. 4, p. 046310, Oct. 2012, doi: 10.1103/PhysRevE.86.046310.

[11] B. Kim, S. Choi, V. S. Pham, R. Kwak, and J. Han, "Energy efficiency enhancement of electromembrane desalination systems by local flow redistribution optimized for the asymmetry of cation/anion diffusivity," *J. Memb. Sci.*, vol. 524, no. July 2016, pp. 280–287,

Feb. 2017, doi: 10.1016/j.memsci.2016.11.046.

[12] S. V. Pham, H. Kwon, B. Kim, J. K. White, G. Lim, and J. Han, "Helical vortex formation in three-dimensional electrochemical systems with ion-selective membranes," *Phys. Rev. E*, vol. 93, no. 3, p. 033114, Mar. 2016, doi: 10.1103/PhysRevE.93.033114.

[13] R. Kwak, V. S. Pham, B. Kim, L. Chen, and J. Han, "Enhanced Salt Removal by Unipolar Ion Conduction in Ion Concentration Polarization Desalination," *Sci. Rep.*, vol. 6, no. 1, p. 25349, May 2016, doi: 10.1038/srep25349.

[14] V.-S. Pham and D.-A. Van, "Numerical modeling for 3D vortices patterns of electroconvective flow developing in shear flow," *Phys. Fluids*, vol. 34, no. 8, Aug. 2022, doi: 10.1063/5.0100731.

[15] D. T. Nguyen and V.-S. Pham, "Ions transport in electromembrane desalination: A numerical modeling for the return flow ion-concentration-polarization desalination system," *Chem. Eng. Res. Des.*, vol. 184, pp. 366–377, Aug. 2022, doi: 10.1016/j.cherd.2022.06.013.